Published in final edited form as:

IEEE Trans Appl Supercond. 2015 June ; 25(3): . doi:10.1109/tasc.2014.2363496.

A High-Resolution 1.3-GHz/54-mm LTS/HTS NMR Magnet

Yukikazu Iwasa, **Juan Bascuñán**, **Seungyong Hahn**, **John Voccio**, **Youngjae Kim**, **Thibault Lécrevisse**, **Jungbin Song**

Francis Bitter Magnet Laboratory (FBML) of the Plasma Science and Fusion Center (PSFC), Massachusetts Institute of Technology (MIT), Cambridge, MA 02139 USA

K. Kajikawa

Francis Bitter Magnet Laboratory (FBML) of the Plasma Science and Fusion Center (PSFC), Massachusetts Institute of Technology (MIT), Cambridge, MA 02139 USA He is now with Kyushu University, Fukuoka 812-8581, Japan.

Abstract

A high-resolution 1.3-GHz/54-mm low-temperature superconducting/high-temperature superconducting (HTS) nuclear magnetic resonance magnet (1.3 G) is currently in the final stage at the Massachusetts Institute of Technology Francis Bitter Magnet Laboratory. Its key component is a three-coil (Coils 1–3) 800-MHz HTS insert comprising 96 no-insulation (NI) double-pancake coils, each wound with a 6-mm-wide GdBCO tape. In this paper, after describing the overall 1.3-G system, we present innovative design features incorporated in 1.3 G: 1) an NI winding technique applied to Coils 1–3 and its adverse effect in the form of charging time delay; 2) persistent-mode HTS shims; 3) a “shaking” magnet; and 4) preliminary results of Coil 1 operated at 4.2 K.

Index Terms

High-temperature superconducting (HTS) shim coils; inside-notch double-pancake (DP) coil; low-temperature superconducting (LTS)/HTS nuclear magnetic resonance (NMR) magnet; screening-current-induced field (SCF) shaking magnet

I. INTRODUCTION

IN NUCLEAR magnetic resonance (NMR), the well-known advantages of higher magnetic field are improved resolution and higher sensitivity. This enables the examination of complex molecular systems such as proteins in a much shorter time frame or with smaller quantities of material. Most solution NMR experiments utilize the TROSY effect to optimize the resolution of the experiments. Initially, it was *predicted* that TROSY experiments would be optimal at ~900 MHz. However, more recent *experimental data* on several proteins indicate that the resolution is optimized in the range of 1200–1400 MHz[1]. In magic-angle-spinning solid-state NMR, the optimal field is simply the highest field available [2]. This 1.3-GHz NMR magnet is expected to become a significant resource for the entire NMR community.

iwasa@jokaku.mit.edu.

From the outset in 1999 when we proposed a three-phase project to build a high-resolution 1-GHz NMR low-temperature superconducting (LTS)/high-temperature super-conducting (HTS) magnet (1 G) to the National Institutes of Health (NIH) [3], our design philosophy for a ≥1-GHz NMR magnet is based on the following key decisions: 1) a combination of an LTS magnet and an HTS insert; and 2) all HTS inserts to be assemblies of double-pancake (DP) coils: 50-MHz (Phase 1) [4], [5] and 100-MHz (Phase 2) [6]–[9], both of Bi2223 tape. At the beginning of Phase 3 of this 1 G project, when, upon recommendation by the NIH, the frequency goal was raised to 1.3 GHz, we decided on a combination of a 700-MHz LTS NMR magnet and a 600-MHz HTS insert (H600), two nested coils of REBCO (Coil 1) and Bi2223 (Coil 2) [10], [11]. In 2012, after a theft, in late 2011, of a nearly completed H600, two versions were considered: first, a 700-MHz GdBCO-Bi2223 insert, i.e., H700 [12], and later the H800 [13]. In December 2012, we adopted a combination of a 500-MHz LTS NMR magnet (L500), already available in the Francis Bitter Magnet Laboratory, and H800 to complete a high-resolution 1.3-GHz LTS/HTS NMR magnet (1.3 G). Note that our 1.3 G relies on a greater field contribution of an HTS insert than an LTS magnet: 18.79 T versus 11.74 T.

II. INNOVATIVE DESIGNS IN H800

The following innovative designs are embodied in H800.

NI Winding Technique

A no-insulation (NI) winding technique [14]–[18] is applied to all DP coils in H800. Its effect on Coils 1–3 are discussed later.

Inside-Notch Pancake Coil

Generally, the longer the overall height of a magnet, the better its inherent field homogeneity [19]. Therefore, to compensate H800, which is shorter than the original H600, those DP coils in the H800 located at the center region are “inside-notched”—the very first this classic field-homogeneity-enhancing technique is deployed to HTS DP coils.

Persistent-Mode HTS Shim Coils (Shims)

The room-temperature bore of a superconducting magnet is magnetically shielded by the “diamagnetic walls” of its own coils. To ameliorate field shimming in our 1.3 G, we have been developing a new shimming technique that relies on a wide YBCO tape. Specifically, persistent-mode HTS shims [20] will be placed in narrow annular space between the liquid helium (LHe) bore tube and Coil 1 innermost winding diameter. This will be discussed later.

“Shaking” Magnet A

“shaking magnet” [21]–[28] to reduce the error fields generated by screening-current-induced field (SCF) [7], [29]–[33] will be installed in the 1.3 G. A design for our 1.3 G based on the performance of a shaking magnet [33] will be presented later.

LHe Recondensation

To mitigate the rising cost of LHe, which is expected to continue for the unforeseeable future, the1.3 G, operated at 4.2 K in a bath of LHe, will be equipped with an LHe recondenser [34].

III. OVERALL SYSTEM

The 1.3 G comprises the L500 and H800; its overall to-scale schematic drawing is shown in Fig. 1. The key components of the 1.3 G are indicated in the figure: L500; H800; HTS shims, Z1, Z2, X, Y; Bi2223-wound SCF shaking magnet. Before discussing the NI technique, presenting designs of HTS shims, a design of shaking magnet, and 4.2-K results of Coil 1, we present below key parameters of L500, H800, and GbBCO tape, including its properties.

L500

This persistent-mode 500-MHz MRI magnet can be operated in the temperature range 4.2–6 K [35]. It chiefly consists of Nb_3Sn coils. The key parameters are listed in Table I. In the previous runs, it never quenched.

H800

Table II lists its key parameters.

GdBCO

Each coil is wound with SuperPower GdBCO coated tape: 6 mm wide and 75 μm thick, of which the Hastelloy substrate is 50 μm thick, and the 5-μm-thick remainder comprises a 1-μm-thick GdBCO layer and other materials. A 10-μm-thick copper layer is electroplated over the entire surface. Table III summarizes the parameters and properties of the GdBCO tape. It also includes those of a G10 spacer between pancake coils.

IV. NI PANCAKES FOR H800 COILS 1–3

The NI winding technique targeted to HTS DP coils was developed in 2011 [14]. Its beneficial features, briefly described below, are viable to H800. Its distinct phenomenon, i.e., charging current delay, is also discussed.

Compact

The H800 is compact. As seen from a top view of the H800 three-coil assembly [see Fig. 2(a)], each NI coil has a radial build markedly smaller than those of the H600, whose two-coil top view is shown in Fig. 2(b). This drastic change is not due to leaving out insulation layers, each ~25 μm thick, but removal of a 225-μm-thick copper strip (one side insulated) from the inner coil of H600, necessitated to prevent overheating as the current commutation option, available in NI winding, is unavailable.

Mechanical

Elimination of mechanically weak organic insulation makes each coil a metallic robust entity.

Self-Protecting

When a normal zone appears in an NI coil, the azimuthal current in the coil quickly switches to the adjacent turns to keep the hot spot from overheating: The NI coil is self-protecting. In an L500 quench, when its current decays over a few minutes, H800 is *globally* driven normal by its induced radial current. Even if the H800 absorbs the entire1.3-G magnetic energy of 6.4 MJ—highly unlikely—it will be heated only to ~280 K. Here, this radial current heats up the built-in resistive elements distributed throughout the NI winding: It *benefits* protection.

Charging Delay and Circuit Model

When an NI DP coil is energized, because current also flows radially, the coil field trails its supply current, characterized by a charging delay time constant, τ_{d}, estimable by an equivalent circuit model. *Each j*th pancake coil of a DP coil is modeled by a parallel L_jR_j circuit[14]–[16]. A circuit model for an NI DP coil comprising $2n_p$ turns is a $2n_p$-series-connected L_jR_j circuit. L_j and R_{j} may be lumped into inductance L_{dp} and resistance R_{dp}, where L_{dp} is the coil inductance, and R_{dp} is the sum of $2n_p$ and R_j [14]–[16]. For an **NI** magnet of N_m DP coils, its L_m is the magnet inductance, and R_m is the sum of N_m and R_{dp}. Thus

$$R_m = \frac{N_m(2n_p)R_c}{[\ell_m w / N_m(2n_p)]} = \frac{4N_m^2 n_p^2 R_c}{\ell_m w} \tag{1}$$

$$\tau_d = \frac{L_m}{R_m}. \tag{2}$$

In (1), R_c is the turn-to-turn *contact resistivity* [$\Omega\,\mathrm{m}^2$]. Fig. 3 shows measured τ_{d} for 26 DP coils in Coil 1, extracted from the $V(I)$ trace of each DP coil; Coil 1 DP coils have an average Ω_{d} of 31 s. With an average self-inductance of 21 mH for these DP coils, we compute R_m =26 × (21 mH/31 s)=17.6 mΩ, or from (1) R_c =35 $\mu\Omega\,\mathrm{cm}^2$, agreeing with those of other GdBCO pancakes [13], and τ_{m} =138 s [(2)] for Coil 1. For Coils 2 and 3, we use the same R_c =35 $\mu\Omega\,\mathrm{cm}^2$ and apply (1) and (2) to compute R_m and τ_{m}—see Table III for N_m, n_p, l_{m}. Computed R_m and τ_{m} for Coils 2 and 3 are, respectively, 9.1 and 6.1 mΩ, and 624 and 603 s. We estimate that it will take ~1 h to energize H800 to 251.3 A.

V. HTS SHIMS: Z1, Z2, X, Y FOR 1.3 G

For a shim placed outside of an HTS magnet, apart from being at a great distance from the magnet center, more crucially, its field is *attenuated* and *distorted* by the *diamagnetic wall* of the magnet [20]. Because H800 represents a diamagnetic wall, superconducting shims *must* be placed in annular space inside its Coil 1 *bore*, where the field is 30.5 T: Only shims of

HTS and a *thin radial build* are viable. We have developed such HTS shims cut from a wide (currently 46 mm and later 100 mm for 1.3 G) YBCO tape, 80-μm-thick overall with a 1-μm-thick YBCO film.

Primarily due to very limited space available to these thin HTS shims (each ~1-mm overall thick), they are not expected to be the only field shimming technique to make this 1.3 G of high resolution. The HTS shims, instead, are to complement conventional RT and ferromagnetic shims. In addition, because they themselves generate error fields, they must be optimized to enhance its benefits and minimize their error field. Fig. 4 shows drawings of ideal (zero thickness) Z1 (a) and X (b) shims, possible with wide YBCO tape. The drawings show proper dimensions in terms of the shim radius, i.e., a. The 1.3 G will have Z1, Z2, X, Y shims in the radius range of 41–43 mm, i.e., each with a 1-mm radial build.

VI. "SHAKING" MAGNET FOR 1.3 G

For a > 1-GHz NMR magnet, similar to our 1.3 G, that must incorporate an HTS insert, SCF, equivalent to magnetization, is a major error field [7], [29], [30]. Although SCF error field is much less serious with LTS magnets than with HTS magnets, a remedy to remove an SCF error field, proposed in 1982 for LTS magnets [21]–[23], also applies to HTS magnet [24]–[28]. The largest SCF error field occurs in the top and bottom end regions of a magnet, where the radial fields, applied and self field, are greatest, and the effective superconductor size approaches the tape width, i.e., 6 mm for H800. The ± screening currents flow in the ± azimuthal directions, separated ± by the tape width. The basic idea is to apply a small time-varying ± axial field, and repeatedly ("shake") force the SC in the radial ± directions, gradually de-pin and wipe out the SCF [26]. Using this shaking field technique, we performed an experiment [33] to confirm that the technique would be applicable to reduce SCF error fields from H800. Fig. 5 shows a shaking field time function, i.e., $B_{sh}(t)$, which is a series of full triangle waves.

The key important results from our experiment are that SCF error field at the magnet center decreases with 1) the number of cycles and 2) B_{sh} amplitude. Equally important is that this decrease in SCF error field is not due to ac losses. We demonstrated this important independence on ac losses by varying shaking field frequency and showing that for a given B_{sh} amplitude, the error field decreases only with the number of cycles.

Table IV lists key parameters of a shaking magnet for 1.3 G. The shaking magnet will be wound with Bi2223/stainless-steel tape, overall 4.3 mm wide and 0.31 mm thick, manufactured by Sumitomo Electric. Fig. 6 shows computed SCF axial field versus axial distance plots from Coils 1–3 at 30.5 T, before and after a shaking field of 60 mT is applied. Although an amplitude of 60 mT (by Coil 1) is 2000 ppm of 30.5 T, because the SCF fields are symmetric about the midplane, their contributions to error fields are zero. However, in reality, a 2000-ppm raw SCF field may generate an error field of ~200 ppm, which may be wiped out by a shaking field of 60 mT, resulting in a total SCF-error field of ~20 ppm. For the NI H800, a full triangular wave period will be 4 h (four ramps, each 1 h long). For 100 cycles, a shaking period will last 400 h or ~17 days.

VII. OVERALL FIELD SHIMMING FOR 1.3 G

Fig. 7 shows a schematic drawing of a field shimming strategy to be deployed to 1.3 G to make its field suitable for a high-resolution NMR magnet. The LTS (NbTi) shims are built into L500 and make L500 by itself of high resolution. The SCF shaking magnet cuts down the H800 SCF error fields to ~20 ppm. Next, the persistent-mode HTS shims (Z1, Z2, X, Y) will bring it to < 10 ppm. Final shimming will be achieved with a combination of RT shims and ferro shims, making 1.3 G of high resolution, i.e., error fields < 0.1 ppm over a 10-mm DSV.

VIII. TEMPORAL FIELD STABILITY

The H800 will be in driven mode, powered by a stable supply. A frequency-locking field-stabilizing technique enabled a driven-mode NMR magnet [34] achieve a temporal field stability of < 0.1 ppm/h; it will be applied to our 1.3 G.

IX. 4.2-K OPERATION OF H800 COIL 1

Coil 1 of H800 was assembled with 25 splices between adjacent pancakes. Fig. 8 shows a photo of Coil 1 before each pancake was overbanded. It was operated at 77 and 4.2 K. To generate a design field of 8.646 T, the coil required a current of 253 A, slightly greater than a design current of 251.3 A. At 4.2 K, the critical currents of 26 DP coils were above 253 A. An average joint resistance at 4.2 K of 26.3 nΩ is nearly half that expected [41]. There seems to be no correlation in resistances between 77 and 4.2 K.

X. CONCLUSION

A key component of a 1.3-GHz/54-mm LTS/HTS NMR magnet (1.3 G) is an 800-MHz GdBCO insert (H800) comprising 96 NI DP coils. The innovative designs, some of their features, and preliminary results presented here and incorporated *for the very first time* in this high-field HTS insert—NI winding technique; inside-notch pancakes; persistent-mode HTS shims; shaking magnet—promise to make 1.3 G a high-resolution NMR magnet. Note that 1.3 G more than any other > 1-GHz LTS/HTS NMR magnets now under development takes advantage of the enabling technology of HTS. Its share, by H800, is 61.5% of 30.5 T. We believe that this trend of an HTS insert doing more heavy lifting in the future > 1.3 GHz NMR magnets is inevitable. Thus, it is more critical to further develop innovative field-shimming techniques, some of which, to be applied to 1.3 G, were reported here.

ACKNOWLEDGMENT

The authors would like to thank G. V. Gettliffe (Massachusetts Institute of Technology) and the Francis Bitter Magnet Laboratory visiting scientists, Dr. Y. Chu (National Fusion Research Institute, South Korea), and Prof. D. Miyagi (Tohoku University, Japan) for contributing to the shaking-magnet experiment. They would also like to thank J. Colque and P. Allen for their assistance and the AMSC for the supply of wide YBCO tape.

This work was supported in part by the National Institute of Biomedical Imaging and Bioengineering (NIBIB) and in part by the National Institute of General Medical Sciences (NIGMS).

REFERENCES

[1]. Wagner G, Harvard Medical School, private communication, 2008, 2014.

[2]. Griffin RG, MIT, private communication, 2008.

[3]. Iwasa Y, "Low and high temperature superconducting NMR magnet," R01-RR15034-01, 1999, NIH.

[4]. Bascuñán J, Bobrov E, Lee H, and Iwasa Y, "A low/high-temperature superconducting (LTS/HTS) NMR magnet: Design and performance results," IEEE Trans. Appl. Supercond, vol. 13, no. 2, pp. 1550–1553, 6 2003.

[5]. Lee H, Bascuñán J, and Iwasa Y, "A high-temperature superconducting (HTS) insert comprised of double pancakes for an NMR magnet," IEEE Trans. Appl. Supercond, vol. 13, no. 2, pp. 1546–1549, 6 2003.

[6]. Bascuñán J et al., "An LTS/HTS NMR Magnet Operated in the range 600–700 MHz," IEEE Trans. Appl. Supercond, vol. 17, no. 2, pp. 1446–1449, 6 2007.

[7]. Hahn S et al., "Field mapping, NMR lineshape, screening currents induced field analyses for homogeneity improvement in LTS/HTS NMR magnets," IEEE Trans. Appl. Supercond, vol. 18, no. 2, pp. 856–859, 6 2008. [PubMed: 31889773]

[8]. Hahn S et al., "Development of a 700 MHz low-/high-temperature superconductor for nuclear magnetic resonance magnet: Test results and spatial homogeneity improvement," Rev. Sci. Instrum, vol. 79, no. 2, 2 2008, Art. ID. 26105.

[9]. Hahn S et al., "Operation and performance analyses of 350 and 700 MHz low-/high-temperature superconductor nuclear magnetic resonance magnets: A march toward operating frequencies above 1 GHz,"J. Appl. Phys, vol. 105, no. 2, 1 2009, Art. ID. 024501.

[10]. Hahn S, Bascuñán J, Yao W, and Iwasa Y, "Two HTS Options for a 600 MHz Insert of a 1.3 GHz LTS/HTS NMR Magnet: YBCO and BSCCO," Phys. C Supercond, vol. 470, no. 20, pp. 1721–1726, 11 2010.

[11]. Bascuñán J, Hahn S, Park DK, Kim Y, and Iwasa Y, "On the 600 MHz HTS insert for a 1.3 GHz NMR magnet," IEEE Trans. Appl. Supercond, vol. 22, no. 3, 6 2012, Art. ID. 4302104.

[12]. Bascuñán J, Hahn S, Kim Y, and Iwasa Y, "A new high-temperature superconducting (HTS) 700-MHz insert magnet for a 1.3-GHz LTS/HTS NMR magnet," IEEE Trans. Appl. Supercond, vol. 23, no. 3, 6 2013, Art. ID. 4400304.

[13]. Bascuñán J, Hahn S, Kim Y, Song J, and Iwasa Y, "18.8-T/90-mm All-GdBCO insert for a 1.3 GHz LTS/HTS NMR magnet: Design and double-pancake coil fabrication," IEEE Trans. Appl. Supercond, vol. 24, no. 3, 6 2014, Art. ID. 4300904.

[14]. Hahn S, Park DK, Bascuñán J, and Iwasa Y, "HTS pancake coils without turn-to-turn insulation," IEEE Trans. Appl. Supercond, vol. 21, no. 3, pp. 1592–1595, 6 2011.

[15]. Hahn S, Park DK, Voccio J, Bascuñán J, and Iwasa Y, "No-insulation (NI) HTS inserts for > 1 GHz LTS/HTS NMR magnets," IEEE Trans. Appl. Supercond, vol. 22, no. 3, 6 2012, Art. ID. 4302405.

[16]. Wang X et al., "Turn-to-turn contact characteristics for an equivalent circuit model of no-insulation Re[RE]BCO pancake coil," Supercond. Sci. Technol, vol. 26, no. 3, 2013, Art. ID. 035012.

[17]. Hahn S et al., "No-insulation coil under time-varying conditions: Charging delay and magnetic coupling," IEEE Trans. Appl. Supercond, vol. 23, no. 3, 6 2013, Art. ID. 4601705.

[18]. Hahn S et al., "No-insulation multi-width winding technique for high temperature superconducting magnet," Appl. Phys. Lett, vol. 103, no. 17, 10 2013, Art. ID. 173511.

[19]. Iwasa Y, Case Studies in Superconducting Magnet, 2nd ed. New York, NY, USA: Springer-Verlag, 2009.

[20]. Iwasa Y et al., "Persistent-mode high-temperature superconductor shim coils: A design concept and experimental results of a prototype Z1 high-temperature superconductor shim," Appl. Phys. Lett, vol. 103, no. 5, 7 2013, Art. ID. 052607.

[21]. Funaki K and Yamafuji K, “Abnormal transverse-field effects in nonideal type II superconductor I. A linear array of monofilamentary wires,” Jpn. J. Appl. Phys, vol. 21, no. 2, pp. 299–304, 1982.

[22]. Funaki K, Nidome T, and Yamafuji K, “Abnormal transverse-field effects in nonideal type II superconductor II. Influence of dimension ratios in a superconducting ribbon,” Jpn. J. Appl. Phys, vol. 21, no. 8, pp. 1121–1126, 8 1982.

[23]. Funaki K, Noda M, and Yamafuji K, “Abnormal transverse-field effects in nonideal type II superconductor III. A theory for an AC-induced decrease in the semi-quasistatic magnetization parallel to a DC bias field,” Jpn. J. Appl. Phys, vol. 21, no. 11, pp. 1580–1587, 11 1982.

[24]. Brandt EH and Mikitik GP, “Why an ac magnetic field shifts the irreversibility line in type-II superconductors,” Phys. Rev. Lett, vol. 89, no. 2, 6 2002, Art. ID. 027002.

[25]. Mikitik GP and Brandt EH, “Theory of the longitudinal vortex-shaking effect in superconducting strips,” Phys. Rev, vol. B67, no. 10, 3 2003, Art. ID. 104511.

[26]. Brandt EH and Mikitik GP, “Shaking of the critical state by a small transverse ac field can cause rapid relaxation in superconductors,” Super-cond. Sci. Technol, vol. 17, no. 2, pp. S1–1–S1–4, 2 2004.

[27]. Kajikawa K and Funaki K, “A simple method to eliminate shielding currents for magnetization perpendicular to superconducting tapes wound into coils,” Supercond. Sci. Technol, vol. 24, no. 12, 12 2011, Art. ID. 125005.

[28]. Kajikawa K and Funaki K, “Reduction of magnetization in windings composed of HTS tapes,” IEEE Trans. Appl. Supercond, vol. 22, no. 3, 6 2012, Art. ID. 4400404.

[29]. Gu C, Qu T, and Han Z, “Measurement and calculation of residual magnetic field in a Bi2223/Ag Magnet,” IEEE Trans. Appl. Supercond, vol. 17, no. 2, pp. 2394–2397, 6 2007.

[30]. Amemiya N and Akachi K, “Magnetic field generated by shielding current in high T_C superconducting coils for NMR magnets,” Supercond. Sci. Technol, vol. 21, no. 9, 9 2008, Art. ID. 095001.

[31]. Ahn MC et al., “Spatial and temporal variations of a screening current induced magnetic field in a double-pancake HTS insert of an LTS/HTS NMR magnet,” IEEE Tran. Appl. Supercond, vol. 19, no. 3, pp. 2269–2272, 6 2009.

[32]. Yanagisawa Y et al., “Effect of YBCO-coil shape on the screening current-induced magnetic field intensity,” IEEE Trans. Appl. Supercond, vol. 20, no. 3, pp. 744–747, 6 2010.

[33]. Kajikawa K et al., “Design and tests of compensation coils to reduce screening currents induced in HTS coil for NMR magnet,” presented at the 23rd Int. Conf. Magnet Technol, Boston, MA, USA, 7 2013.

[34]. Yanagisawa Y et al., “Operation of a 500 MHz high temperature superconducting NMR: Towards an NMR spectrometer operating beyond 1 GHz,” J. Magn. Resonance, vol. 203, no. 2, pp. 274–282, 4 2010.

[35]. Bascuñán J, Hahn S, Ahn M, and Iwasa Y, “Construction and test of a 500 MHz/200 mm RT bore solid cryogen cooled Nb_3Sn MRI magnet,” Adv. Cryogenic Technol, vol. 55A, pp. 523–530, 4 2010.

[36]. Kasaba K et al., “Stress/strain dependence of critical current in Nb_3 Sn superconducting wires stabilized with CuNb microcomposites—Effect of Nb content,” Cryogenics, vol. 41, no. 1, pp. 9–14, 1 2001.

[37]. Lu J, Choi ES, and Zhou HD, “Physical properties of Hastelloy c – 267™ at cryogenic temperatures,” J. Appl. Phys, vol. 103, no. 6, 3 2008, Art. ID. 064908

[38]. Reed RP and Clark AF, Materials at Low Temperatures. Metals Park, OH, USA: American Society for Metals, 1983.

[39]. Hazelton D, “Application of SuperPower 2 G HTS wire to high field devices,” presented at the 22nd Int. Conf. Magnet Technol, Marseille, France, 9 12–16, 2011.

[40]. [Online]. Available: hhtp:/www.k-mac-plastics.net/data%20sheets/fiberglass_technical_data.htm

[41]. Lécrevisse T et al., “Pancake–pancake joint resistances of a magnet assembled from GdBCO double-pancake coils,” presented at the 23rd Int. Conf. Magnet Technol., Boston, MA, USA, 7 14–19, 2013.

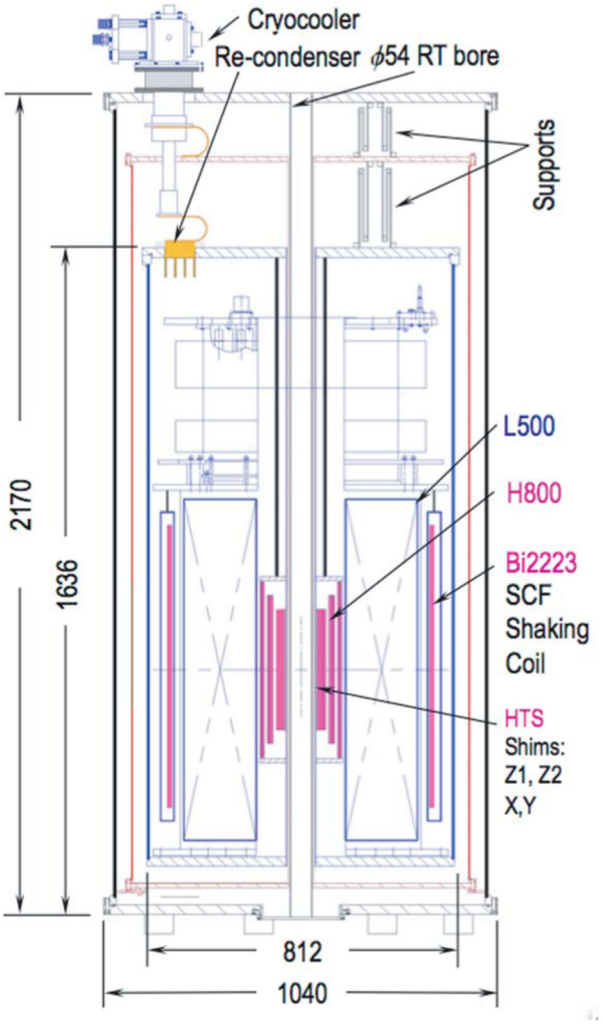

Fig. 1.
Cross section of 1.3 G.

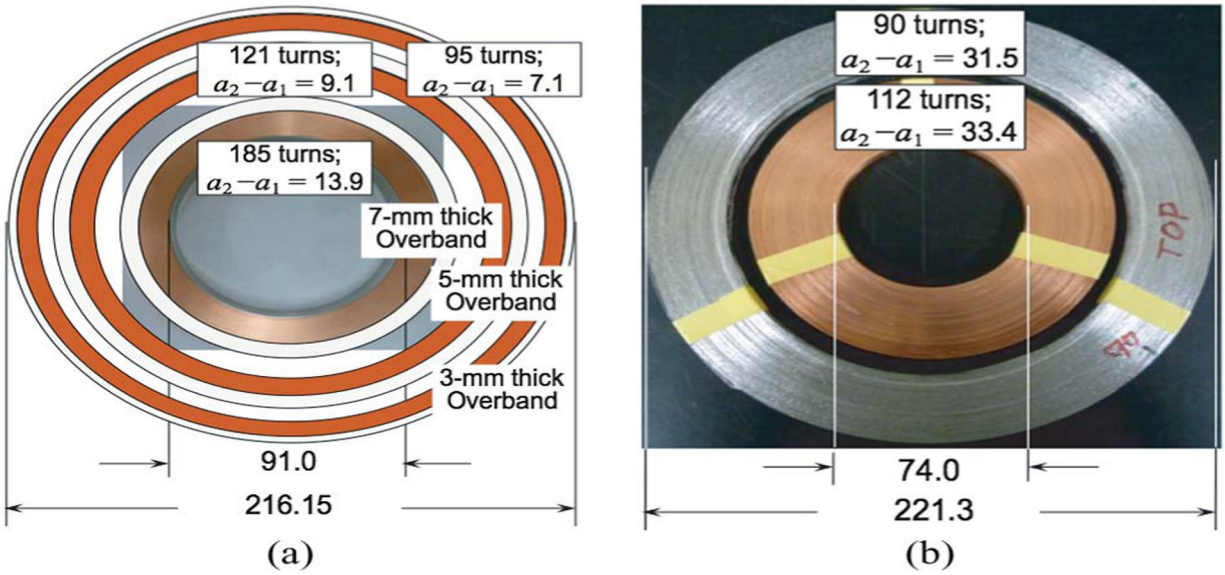

Fig. 2.

(a) Three-NI-coil H800: Coil 1 and Coils 2 and 3 (drawings), all 6-mm-wide GdBCO tape. (b) Original two-coil H600 (photo): inner, *insulated* 4-mm-wide GdBCO tape cowound with 225-μm-thick Cu tape; outer 4.3-mm-wide Bi2223 tape. Dimensions are in millimeters.

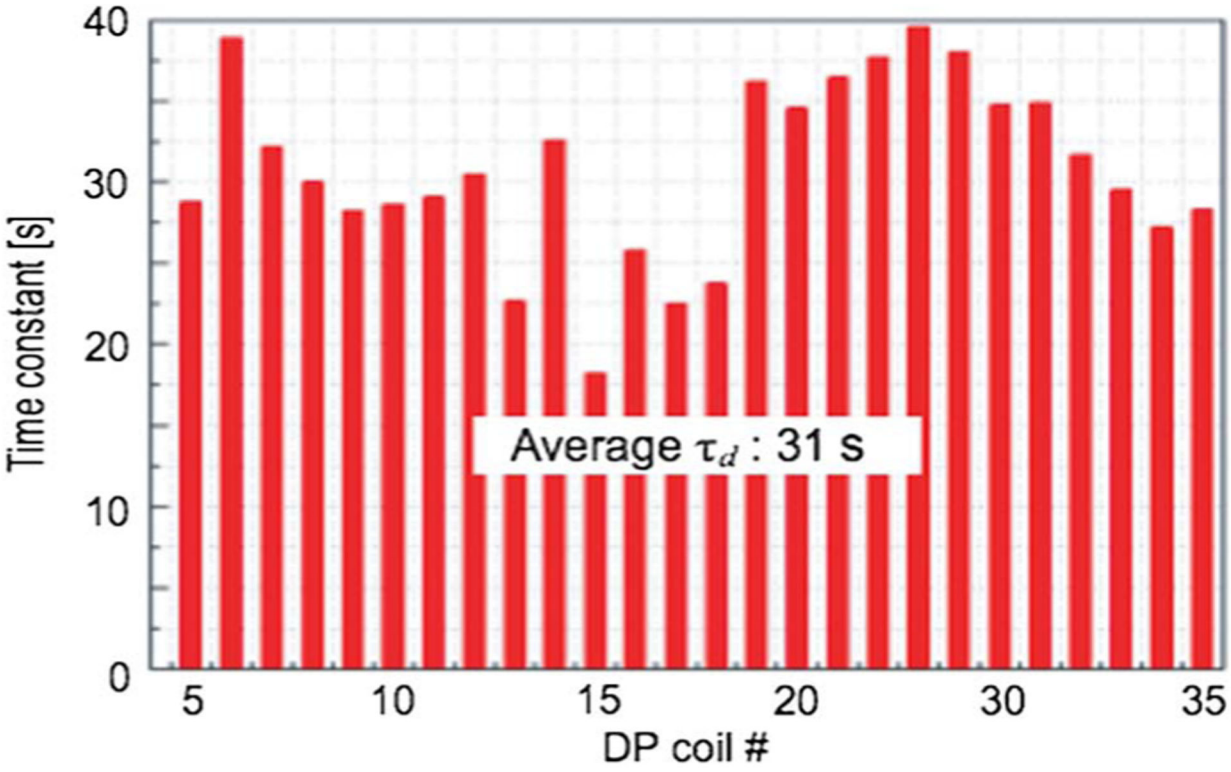

Fig. 3.
τ_d for Coil 1 26 DP coils.

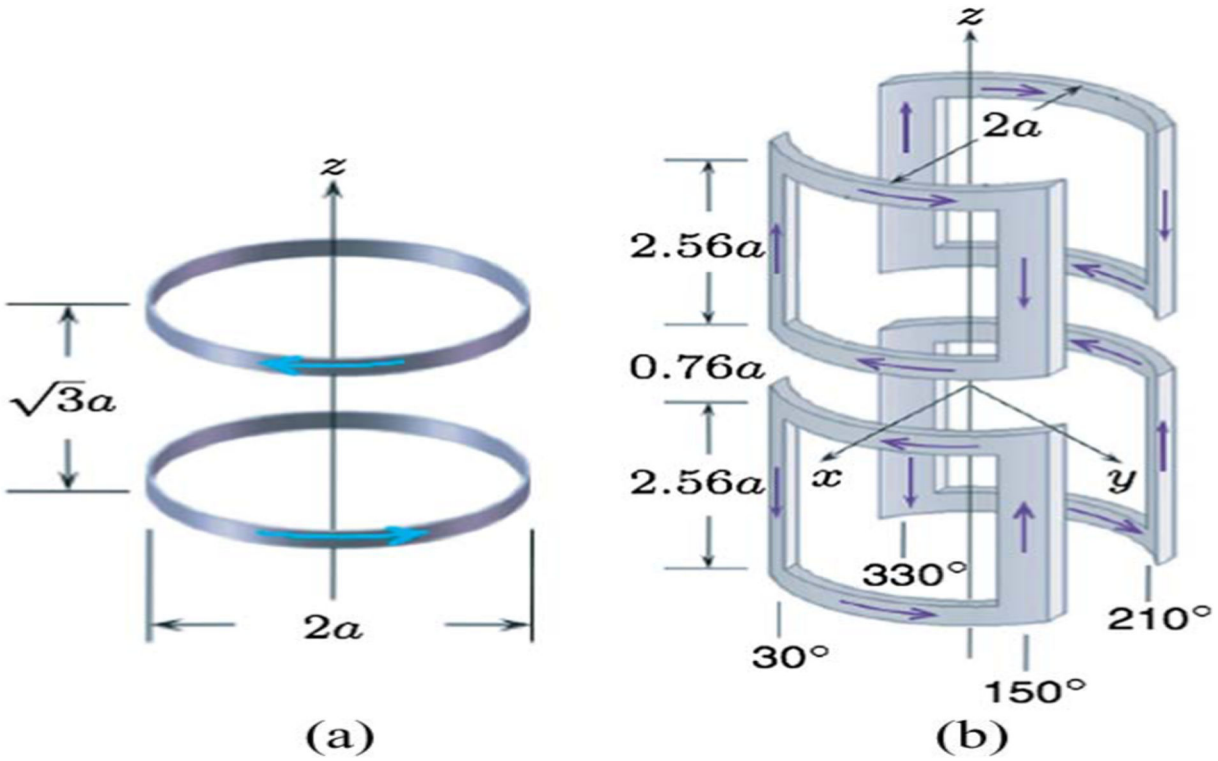

Fig. 4.
Ideal (a) Z1 and (b) X shims.

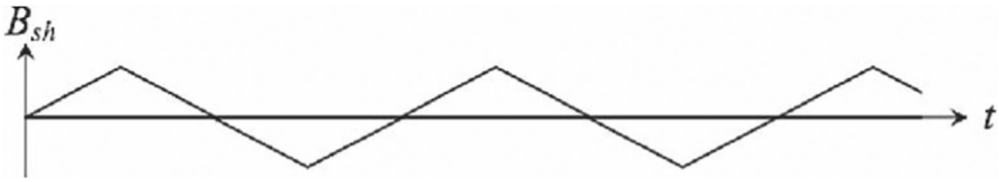

Fig. 5.
Time function of shaking magnetic field.

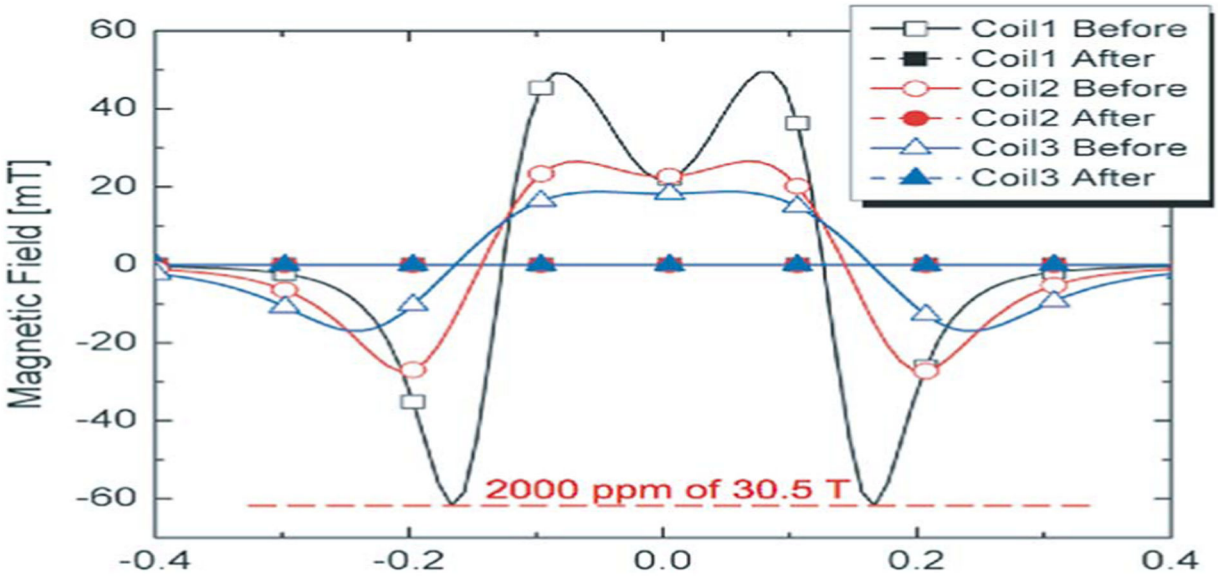

Fig. 6.

Computed axial Coils 1–3 SCF plots versus axial distance at 30.5 T before and after a ±60-mT shaking field (see Table IV).

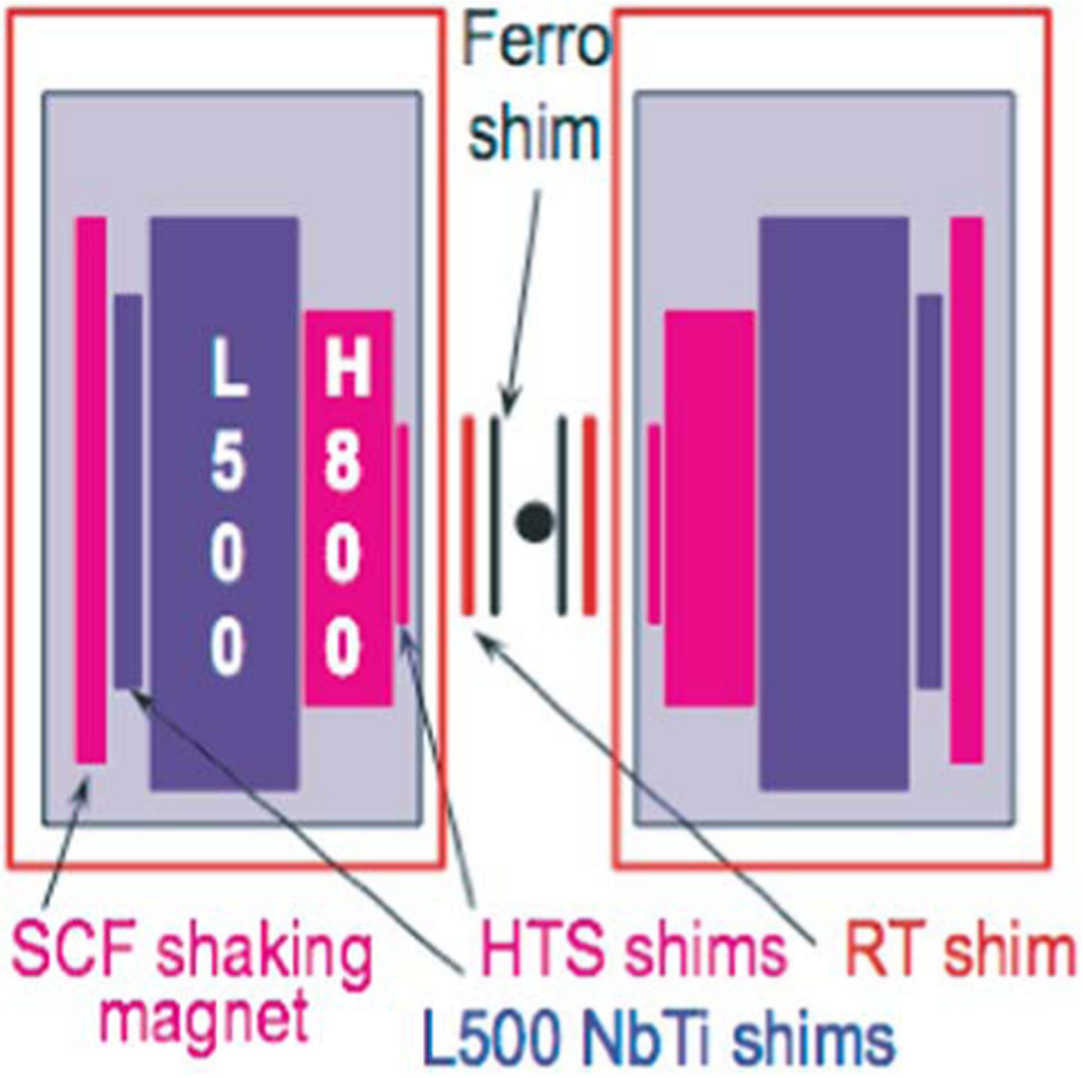

Fig. 7.
1.3 G field shimming.

Fig. 8.
Photo of Coil 1 before overbanded.

TABLE I

L500 (11.74 T)

Operating temperature	[K]	4.2–6.0
Cold bore for H800	[mm]	237
Over all diameter; height	[mm]	780;1422
Magnet mass	[kg]	1200
Magnetic energy @ I_{op}=246 A.	[MJ]	4.6
Temporal stability	[ppm/hr]	< 0.01
Measured field homogeneity	[ppm]	0.45 *

* 17-mm diameter × 30-mm length.

TABLE II

H800 (18.79 T) IN L500 AT 4.2 K

Parameter		**Coil1**	**Coil2**	**Coil3**
Frequency/field	[MHz/[T]]	369/8.66	242/5.68	189/4.44
I_c *@77K, self field (sf)*	[A]		> 160	
$B_\perp$	[T]	4.8	4.6	3.7
$I_c(B_\perp,4.2K)/I_c(77K,sf)$		> 2.3	> 2.3	> 2.7
Operating current/density	[A]/[MA/m^2		251.3/546.9	
Total # DP coils (notched)		26(6)	32(8)	36(8)
# turns/pancake		185.1	121	95
# turns/notched pancake		176.6	118	93
Winding i.d.	[mm]	91.0	150.7	195.9
Winding i.d. (notch)	[mm]	92.4	151.2	197.2
Winding o.d.	[mm]	117.6	167.9	210.1
Windingn overall height	[mm]	323.7	392.1	465.7
Notched section height	[mm]	74.7	122.5	98.0
SS overband radial build	[mm]	7	5	3
GdBCO length/DP	[m]	121.9	121.5	121.8
GdBCO length/notch DP	[m]	116.7	118.7	119.3
Total length/Coil	[km]	3.14	3.84	4.61
Inductance	[H]	2.43	3.08	3.71
Peak bending strain	[%]	0.060	0.036	0.028
Peak magnetic hoop strain	[%]	0.41	0.35	0.32
Peak total hoop strain	[%]	0.47	0.39	0.35
Radial strain	[%]	< −0.1	< −0.1	< −0.1
R_m (Eq.l for Coils 2,3)	[mΩ]	17.6	9.1	9.1
τ_m (Eq.2 for Coils 2,3)	[s]	138	624	603

TABLE III

GDBCO TAPE: PARAMETERS AND PROPERTIES

Non-GdBCO material		Hastelloy	Cu & others
Overall width/thickness	[mm/μm]	6.0/50	6.0/25
I_c *@77K*	[A]	> 160	
Young's modulus (E)	[GPa]	197	33 * [37]
Poisson's ratio (v)		0.33	0.33
α † *(77K→4.2K)*	[%]	0.03 [38]	0.02 [39]
E_r, E_h, E_z,	[GPa]	73;142;134	
Vrh, Vzh, Vrz		0.40; 0.35; 0.18	
α_r, α_h, α_z*(77K→4.2K)*	[%]	0.026; 0.026; 0.030	
95%-I_c strain @77K	[%]	0.6 [40]	
95%-$I_{C\psi}$ stress @77K	[MPa]	> 850	
Pancake-to-pancake 127-μ thick G-10 spacer: v = 0.33 [41]; $E_r = E_h$ = 36 GPa; E_z = 22 GPa [39] $\alpha_r = \alpha_h$ = 0.03 %; α_z = 0.07 % [39]			

* Assumed all Cu: 165MPa and 0.5% strain @4.2K, 14 T [37].

† Thermal contraction: $(l_{77\ \mathrm{k}} - l_{4.2\ \mathrm{k}})/l_{293\ \mathrm{k}}$

TABLE IV

KEY PARAMETERS OF SHAKING MAGNET FOR 1.3 G

		M	C1	C2	C3	C4
Winding $2a_1$ *(i.d.)*	[mm]			600		
Winding $2a_2$ *(o.d.)*	[mm]	602.1	600.7	603.5	600.7	600.7
b_1	[mm]	−48.3	48.3	108.2	158.9	320.0
b_2	[mm]	48.3	108.2	158.9	320.0	407.5
# turns/layer; # layers		21; 3	13; 1	11; 5	35;1	19;9
Total conductor length	[m]			1160		
Magnet inductance	[mH]			126		
B_{sh} *@*I_{op} = 98 A	[mT]			60		
B_{sh} *field error @*I_{op}	[%]			< 0.3(500-mm DSV)		
One wave cycle period	[hr]			4(=1↑+1↓+1↑+1↓)		
Shaking period	[day]			~17 [= (4 hr/cycle) × 100 cycles]		